Key factors explaining severe air pollution episodes in Hanoi during 2019 winter season

Bao Anh Phung Ngoc, Hervé Delbarre, Karine Deboudt, Elsa Dieudonné, Dien Nguyen Tran, Son Le Thanh, Jacques Pelon, François Ravetta

Key factors explaining severe air pollution episodes in Hanoi during 2019 winter season

Bao Anh Phung Ngoc[a,b], Hervé Delbarre[a], Karine Deboudt[a], Elsa Dieudonné[a], Dien Nguyen Tran[b], Son Le Thanh[b], Jacques Pelon[c], François Ravetta[c]

[a] *Laboratoire de Physique et Chimie Atmosphériques (LPCA), Université du Littoral Côte d'Opale, Dunkerque, France.*

[b] *Institute of Environmental Technology (IET), Vietnam Academy of Science and Technology, Hanoi, Vietnam.*

[c] *Laboratoire Atmosphère Milieux, Observations Spatiales (LATMOS), CNRS-INSU, Sorbonne Université, Université Versailles St Quentin, Paris, France.*

*Corresponding author: Bao Anh Phung Ngoc

E-mail addresses: anh-bao.phung-ngoc@univ-littoral.fr

Abstract: With the aim of identifying key factors explaining the severe pollution events that occur under the impact of the Northeast monsoon during the winter period in Hanoi, a two-month campaign was carried out (11 January to 22 March 2019). The local meteorological parameters and the origin of the air masses were investigated, notably using a Doppler Lidar, and the structure of the boundary layer was thoroughly studied using elastic Lidar measurements for the first time in Hanoi. Four heavily polluted events occurred during the campaign, which were associated with hazy days; the highest daily $PM_{2.5}$ concentrations reached ~130 µg m^{-3} while the mean concentration during the campaign was 45 ± 25 µg m^{-3}. These severe polluted events in Hanoi were mainly related to LRT coming from China besides local emission or LRT from other polluted regions of Vietnam. BLH proved to be one of the key factors controlling air pollution in Hanoi. Indeed, the elastic Lidar measurements showed that the daily maximum of the hourly BLH varied from 700m to 1200m during cloudy days, while it was always below 1000m during hazy days. The lower BLH on the hazy days weakened the vertical mixing and was directly related to an increase in aerosol concentrations at the surface.

Keywords: Air pollution; Boundary layer; Southeast Asia ; Haze; Lidar; $PM_{2.5}$

Abbreviations:

AQI: Air Quality Index

BL: Boundary layer

BLH: Boundary layer heights

BAM: Beta attenuation monitoring

RH: Relative humidity

ROCS : Range and overlap corrected signal

SLIM: Aerosol micro-pulse Lidar

SEM-EDX: Scanning Electron Microscopy coupled

with Energy Dispersive X-Ray analysis

CBL: Convective boundary layer

DBS: Doppler Beam Swinging

EPA: U.S. Environmental Protection Agency

GDAS: Global Data Assimilation System

GM: Gradient method

HYSPLIT: Hybrid Single Particle Lagrangian Integrated Trajectory

LRT: Long-Range Transport

LLJ: Low-level jet

NAAPS: US Naval Research Laboratory

NBL: Neutral boundary layer

OS : Observation Site

PM: Particulate matter

SBL: Stable boundary layer

T: Temperature

TSP: Total Suspended Particles

TSV: Total spatial variance

USE: US Embassy

VAST: Vietnam Academy of Science and Technology

VMHA: Vietnam Meteorological and Hydrological Administration

VC: Ventilation coefficient

WS: Wind speed

WD: Wind direction

WAQI: World Air Quality Index

1. Introduction

A high level of particulate matter (PM), especially $PM_{2.5}$ (particles with aerodynamic diameters $\leq 2.5\mu m$), has been proven to adversely impact human health and life quality (Kelly and Fussell, 2012; Pope et al., 2020). Moreover, $PM_{2.5}$ has been considered as the main pollutant causing severe air pollution issues in cities in Southeast Asia (Reddington et al., 2019; Janta et al., 2020) including Hanoi (Cohen et al., 2010a, 2010b; Hai and Kim Oanh, 2013; Ly et al., 2020). Hanoi, the capital of Vietnam, has experienced rapid growth and urbanization over the past two decades along with extreme changes in weather such as atmospheric circulation, air temperature and downward solar radiation (Taylor, 2010; Nguyen et al., 2019), resulting in a severe increase of pollutants such as $PM_{2.5}$, NO_x and SO_2.

From 2010 to 2013, considering the EPA's Air Quality Index (AQI), the number of days with unhealthy levels for sensitive groups (AQI = 101 - 200) accounted for 40 to 60% of the monitored days at Hanoi, while 102 days and 20 days were associated with very unhealthy (AQI = 201 - 300) and hazardous ($AQI \geq 300$) levels, respectively (MONRE, 2013). Concerning PM, the diurnal particulate

concentrations fluctuate substantially along the year. Daily variations of fine ($PM_{2.5}$) and coarse (PM_{10}) particulate matter concentrations in Hanoi varied from 26 to 143 μg m^{-3} and from 37 to 165 μg m^{-3} respectively (Hai and Kim Oanh, 2013). Furthermore, the number of days with levels of PM_{10} exceeding the specified Vietnam's standard for ambient air quality in 24-h (≥ 150 μg m^{-3}) was approximately 50 days per year (Hien et al., 2011) while $PM_{2.5}$ concentrations exceeding standard (≥ 50 μg m^{-3}) were also recorded regularly. As a result, air pollution has been identified as one of the major environmental concerns in Hanoi. Northern Vietnam has two main seasons, which include Winter (November - March) and Summer (May - September), and two transitory seasons Spring including (April) and Autumn (October) (MONRE, 2007). Particularly, PM concentrations in Hanoi are lower in summer, when the southeast monsoon directed by tropical maritime air from the Pacific and Indian Oceans delivers hot weather and convective conditions. Conversely, high levels of PM are recorded in winter, when northern Vietnam is affected by the northeast monsoon (Cohen et al., 2010a; Hien et al., 2011; Huy and Kim Oanh, 2017). Moreover, a high-pressure ridge from polar air in Siberia results in the northeast monsoon bringing continental cold air from this area either through inland China (dry period) from November to January or via the Gulf of Tonkin (humid period) from January to March. However, the synoptic motion of air masses is not the only parameter that can explain the pollution levels encountered in Vietnam. A high level of pollutants was noticed in winter in Hanoi for days under haze condition (Ly et al., 2018, 2020), so the humidity can play a notable role in the variation of pollutants. Besides local emissions, long-range transport (LRT) was also considered as a potential source to the high level of PM, especially in winter with a strong impact of the northeast monsoon. Although there was still a debate, a few studies have stated a similar contribution of emission originating from both local and LRT sources in Hanoi (Cohen et al., 2010a; Nguyen et al., 2020).

On the other hand, boundary layer heights (BLH) and vertical wind profiles also play an important role in the vertical mixing and transport of pollutants (Stull, 1988). Solar radiation and weather conditions are the main variables affecting the dynamics of the boundary layer (BL). Inland, BL may undergo a typical daily evolution driven by surface heating, but it is also strongly dependent on local meteorology (haze, sea-breeze) and fronts (Stull, 1988). Concerning wind profiles, horizontal and vertical wind speeds can change quickly in time as well as in space, thus, monitoring these profiles lead to improve our understanding of atmospheric dynamics as well as the evolution of the BL. Radiosonde measurements are considered as the most reliable method for retrieving vertical profiles of meteorological parameters as well as BLH. Unfortunately, soundings are usually released into the

atmosphere 2 - 3 times per day, so this method is not able to monitor continuously the BLH evolution. Nowadays, Lidar becomes more suitable for analyzing the BL structure and determining BLH due to its high spatio-temporal resolution. However, this method requires greater technical resources and it still has some optical limits especially under cloudy weather. In a few recent decades, Lidar's application in order to analyze the BLH is widely applied in many regions of the world like Europe and Asia (Menut et al., 1999; Delbarre et al., 2005; Dieudonné et al., 2017; Liu et al., 2019; Pan et al., 2019). However, similar studies in Southeast Asia, especially in Vietnam are still limited (Hai et al., 2013).

In this study, our goal is to identify the key factors explaining severe pollution events in Hanoi during winter, which is the highest pollution period over the year. The impact of the local meteorological factors and the origin of the air masses will be firstly investigated. In addition, the structure of BL will be thoroughly studied by the Lidar measurements for the first time in Hanoi. The impact of its evolution as well as of atmospheric dynamics on hourly $PM_{2.5}$ concentrations during pollution episodes will be explored.

2. Field campaign for a dynamical study of air pollution in Hanoi

2.1 Devices, location and availability

The campaign was carried out from 11 January to 22 March 2019 in Hanoi. Three observation sites (OS) located in the urban area were considered (Fig. 1): OS1 located at Vietnam Academy of Science and Technology (VAST) (21° 2' N, 105° 47' E) which is a residential and traffic mixed area including a ring road and several busy roads, OS2 at US embassy (USE) building (21° 1' N, 105° 49' E) and OS3 at Vietnam Meteorological and Hydrological Administration (VMHA) (21° 1' N, 105° 48' E). The surrounding areas of sites OS2 and OS3 are also densely populated and experience busy traffic.

First of all, a Doppler Lidar (Windcube V2 from Leosphere/Vaisala) and a custom-made aerosol micro-pulse Lidar (SLIM) were located at the site OS1 on the rooftop of a 15m high building. In addition, an aerosol sampler was set up next to the Lidar devices. A meteorological station (Davis Instruments, Hayward, CA; model Vantage Pro 2) was placed on the rooftop of a second building (50m above ground level (a.g.l.), around 100m away from the Lidar location) to minimize the impact of high buildings around the site OS1. Next, the site OS2 hosted a $PM_{2.5}$ analyzer, based on a Beta Attenuation Monitoring (BAM) system, from an international monitoring network of the World Air Quality Index (WAQI) at USE. $PM_{2.5}$ concentrations in Hanoi were retrieved from EPA (https://www.airnow.gov/). Finally, the sounding profiles were extracted from the University of Wyoming website (http://weather.uwyo.edu/upperair/sounding.html) and radiosondes are launched routinely from site

OS3 by VMHA twice per day, at 07:00 and 19:00 local time (LT) (i.e. 00:00 and 12:00 UTC). This radiosonde generally offers profiles of temperature, pressure, relative humidity, wind speed and direction with a vertical resolution of 5m.

2.2 Remote sensing of boundary layer and wind vertical profile

2.2.1 Doppler Lidar (Windcube V2)

The Windcube V2 from Leosphere/Vaisala is an eye-safe pulsed Doppler Lidar operating in the infrared (1.543 µm) at low power (7mW laser). It measures the Doppler shift due to the particles motion along the laser beam direction (radial wind speed), which is determined through heterodyne detection followed by fast Fourier transform analysis. The profiles of the three components of the wind are reconstructed using the Doppler Beam Swinging (DBS) technique originally proposed for Doppler radars (Koscielny et al., 1984), here combining four slanted beams (28° from zenith) pointing in the cardinal directions and a vertical beam. The accumulation time is 1s per bream so that a DBS cycle is repeated every 5s; then, wind observations are averaged over 10-min periods. The laser pulse duration and shape allow a 20m vertical resolution while the optics allow a minimal/maximal range of 40/280m a.g.l. During the campaign, this device was set to retrieve the wind every 20m from 60m to 280m a.g.l. (the 40m altitude was not used due to the interference of nearby higher buildings). Besides wind speed (WS) and wind direction (WD) profiles, the vertical wind speed standard deviation (σ_w) was also computed using the Doppler Lidar observations. This quantity provides a direct estimation of the amount of turbulence, thus the vertical mixing state of the BL.

2.2.2 Aerosol micro-pulse Lidar (SLIM)

The SLIM was deployed during the campaign. It is a custom-made micro-pulse Lidar developed at LATMOS in collaboration with CIMEL that operates at the edge of the visible spectrum (808nm) and at low power (12 mW laser). The device was pointed at the zenith and recorded profiles of elastic signal back-scattered by the atmosphere with a vertical resolution of 15m, averaged over 10-min, then 1-h. The overlap function was determined using the slope method applied to a 3-h average profile recorded in a well-mixed afternoon BL. Then, the BLH was determined by the 1-h average profiles of the Range and Overlap-Corrected Signal (ROCS), noted P(z) with the altitude (z).

In cloud-free conditions, the Lidar signal yields a strong back-scattering from the particles within the BL, then decreases through a transition zone and disperses completely in the free troposphere as back-scattering from the molecules is much weaker, especially at 808nm. Thus, the first derivative $dP\,(z)/d\,z$ of the ROCS exhibits a strong negative peak at the height which is considered to be the BLH.

This well-known method for BLH determination is the Gradient Method (GM) (Flamant et al., 1997; Cohn and Angevine, 2000). The GM is still valid when a thin cloud is capping the BL. Indeed, that type of cloud is included in the BL, and the GM will then detect the strong decrease of signal occurring when the laser beam exits the cloud. When a thick cloud is present just above the BL, it rapidly extinguishes the laser beam, and the GM will return the extinction height, which is located inside the cloud. This will cause a slight overestimation of the BLH because thick clouds are not included in the BL, so the cloud base should be considered instead as BL top. However, this slight overestimation is not a problem when the main point is to follow the BLH variability and its influence over pollution, so a simple and more reliable algorithm was preferred. Table A.1 shows the SLIM data availability during the campaign. Due to technical issues as well as problems with water condensation in the optical head, the retrieval-signals in all the days was not always reliable and even if the data were available, it did not mean that processing them to retrieve the aerosol optical properties was always possible.

2.3. Aerosol sampling and elemental analysis

Total Suspended Particles (TSP) were collected at site OS1 by total filtration with 1-week period on cellulose filter (Whatman® grade 41) with a flow rate of 1.2 $m^3 h^{-1}$. The filters were changed every Wednesday at 16:00 LT from 11/01 to 22/03, resulting in 10 TSP samples referenced from S_1 to S_{10}.

One fraction of each filter was dedicated to the analysis of the water soluble NO_3^- and SO_4^{2-} by ionic chromatography, using an ICS 5000+ ion chromatograph from Thermo Scientific Dionex equipped with an anionic CS 12A column (2x250 mm). After leaching of the sample in ultrapure water (18.2 MΩ cm) under ultrasonic shaking for 1-h, the obtained aqueous solution was filtered (IC Millex®, Millipore) and analyzed using KOH solution as eluent. Atmospheric concentration of ammonium is then deduced from nitrate and sulfate concentrations considering atmospheric nitric and sulfuric acids as completely neutralized by ammoniac.

The other fraction of each filter was dedicated to SEM-EDX (Scanning Electron Microscopy coupled with Energy Dispersive X-Ray) analysis using a JEOL™ JSM7100F electron microscope, equipped with three ultrathin-window (30mm^2) energy-dispersive X-ray detectors (Bruker™ XFlash 6/30). EDX spectra were acquired at an acceleration voltage of 15 kV, a probe current of 200 pA with a time acquisition of 40s. 10 spectra per sample were acquired with large fields (1600 x 1100 μm^2) and summed to be then considered as one. Then, the elemental ratios of detected elements (Na, Mg, Al, Si, S, Cl, K, Ca, Ti, Fe, Zn) were calculated using PhiRoZ quantification procedure from

the Esprit Software (Bruker Nano, Germany). The most significant error in the quantitative analyses is due to the heterogeneity of particle deposition on the surface of the collection substrate. To assess this, relative standard deviations associated with the 10 spectra per sample were calculated. They depend strongly on the element considered, but are less than 10% for major elements and up to 20% for minor elements. Atmospheric concentrations were then computed based on the atmospheric SO_4^{2-} concentrations measured by ionic chromatography and S relative content in PM measured by EDX, considering Al, Si, Ti, Fe and Zn as oxides and Ca as calcite. Though the particulate carbon fraction has not been determined, the sum of these compounds represents a large part of the TSP and is highly correlated with the online $PM_{2.5}$ measurements with BAM ($y = 1.22x$, $R^2 = 0.83$).

2.4 HYSPLIT (Hybrid Single Particle Lagrangian Integrated Trajectory) back-trajectories

The PC Windows-based HYSPLIT model (Stein et al., 2015) was widely used for generating backward trajectories to evaluate potential sources for LRT. The Global Data Assimilation System (GDAS) was used as weather input to the HYSPLIT model. 72-h backward trajectories were computed, ending at site OS1 every hour from 11/01 to 22/03/2019. Based on the observation of the radiosonde profiles, four ending altitudes were used: 100m a.g.l. (daytime surface layer or stable layer), 600m a.g.l. (convective layer or residual layer), 1000m a.g.l. (transition layer) and 1500m a.g.l. (free troposphere).

Single backward trajectory estimation by the HYSPLIT model has been considered to be definite, but still maintain some computational uncertainty. For example, 10 to 20% of the travel distance was estimated as the horizontal uncertainty of the trajectory measurements (Draxler and Hess, 1998), while the bias of trajectories originated from wind fields considered to be typically of the order of 20% of the travel distance (Stohl, 1998). However, the accuracy of this model can be improved by using a large number of trajectories in statistical analysis (Cabello et al., 2008). Thus, control measures were applied in our study to improve confidence in the HYSPLIT generated back-trajectories: Firstly, trajectories were computed for four different heights to reduce topographic effects as well as to sample the different dynamic layers. Secondly, an 1h integration time step, which is the shortest possible in HYSPLIT, was used for the cluster analysis. Finally, the statistical analysis with a huge number of trajectories arriving at the study site was performed to reduce the uncertainties of the cluster analysis. In total, almost 1700 backward trajectories were computed and classified using the clustering analysis of the HYSPLIT software. These trajectories were assigned to clusters depending on their characteristics (speed and direction) using a k-means clustering method, which has been considered as one of the simplest

unsupervised learning algorithms. The optimal number of clusters were chosen so as to minimize the total spatial variance (TSV).

3. Results and discussion

3.1 Overview of basic meteorological parameters and pollution during the campaign

A summary of the meteorological conditions and their temporal variability for each month is shown in Table 1. January was colder by ~ 3°C compared to February and March. Since the whole campaign was carried out in the humid period, the RH was high. The visibility was at its lowest in January due to frequent fog/haze episodes, and its highest in February. Moreover, monthly-mean $PM_{2.5}$ concentrations were the highest in January, while the lowest concentrations were recorded in February, probably as a result of the decrease of industrial activity and transport during the Lunar New Year (01 - 10/02). Figure 2 shows the mean $PM_{2.5}$ levels as a function of the WS and WD, using wind data from the Doppler Lidar at 100m a.g.l. as input. This height was chosen to be just above the highest buildings in the area (which have 30 to 35 floors). Besides, the WS from the NE and SE were predominant during the three months, which is typical of the winds observed in winter in Hanoi (Lasko et al., 2018). This figure also explicitly demonstrates that the highest levels of $PM_{2.5}$ were mainly related to weak WS, so probably due to local emissions that are not well dispersed. These local sources seem to be mainly located to the west of site OS1 in January, to the Northeast in February and to the East and Southeast in March. Nevertheless, a finer analysis of the atmospheric dynamics is necessary to draw reliable conclusions on the origin of this pollution.

Table 1: Statistical summary (mean ± one standard deviation) of meteorological parameters for each month.

	January	***February***	***March***
T (°C)	18.3 ± 2.5	21.9 ± 3.2	21.4 ± 2.8
RH (%)	83.1 ± 6.7	85.2 ± 4.9	85.9 ± 7.2
WS (m s^{-1})	3.1 ± 1.2	3.9 ± 0.8	3.5 ± 0.87
Visibility (km)	5.4 ± 2.4	7.1 ± 1.6	6.5 ± 2.1
$PM_{2.5}$ (µg m^{-3})	56.8 ± 33.2	36.4 ± 14.2	44.4 ± 23.5

Figure 3 displays time-series of the daily averages of some basic meteorological factors along with the $PM_{2.5}$ concentrations during the campaign. Figure 3a shows the daily average temperature (T) in a range of 12°C - 26°C. In addition, the weather in this period was under humid conditions with daily relative humidity always higher than 60% (Fig. 3a). This humid condition might facilitate a reinforcement in the level of $PM_{2.5}$ through the formation of secondary aerosols by heterogeneous

reactions and their hygroscopic growth in ambient air (Tang and Munkelwitz, 1994; Marris et al., 2012). This is notably demonstrated by an increase of the sulfate to nitrate ratio retrieved from our weekly PM samples as a function of relative humidity (RH) (Fig. A.1). Indeed, the sulfate can be formed in aqueous phase reaction at high RH, while the nitrate is predominantly formed by gas-phase or heterogeneous photo-chemical reaction (Seinfeld and Pandis, 2006). Figure 3b shows the result of daily-average value of solar radiation (Q) and the daily maximum of the hourly BLH values (max BLH) for each day during the study period. We can observe a relation between these two parameters, but the correlation is very weak ($r^2 = 0.44$) because the weather is often cloudy during the campaign. In conclusion, the solar radiation cannot be a good indicator of the maximum BLH at this period of the year and the BLH need to be measured with a reliable method. Concerning $PM_{2.5}$, the daily values varied from 9 to 129 μg m^{-3} (Fig. 3f) with an average and standard deviation of 45 ± 25 μg m^{-3}, which are typical values recorded in Hanoi within this period (Hien et al., 2011; Huy and Kim Oanh, 2017). The highest daily level of $PM_{2.5}$ was recorded on 25 January (129 μg m^{-3}), while the lowest daily $PM_{2.5}$ concentrations (~ 25 μg m^{-3}) were mainly recorded in February. During the campaign, four heavily polluted events characterized by $PM_{2.5}$ higher than 50 μg m^{-3} for more than 48-h were observed (P1 - P4 marked by grey areas), based on the specified Vietnam's standard for ambient air quality. Although this is not always the case, the daily variation of $PM_{2.5}$ concentration is generally associated with local WS: high WS are related to low concentrations of $PM_{2.5}$ and lower WS correspond to the high levels of $PM_{2.5}$ (Fig. 3c and 3f).

In order to study the relation between PM concentration and meteorology, weather conditions were classified into four distinct types typically observed in Hanoi from January to March: “clear”, “hazy”, “foggy” and “cloudy” conditions (Fig. 3f). In this paper, hazy days should satisfy two criteria: a daily visibility ≤ 5km and a daily RH ≤ 95%. Foggy days were discriminated only by RH ≥ 90%. The clear days were selected by a daily visibility ≥ 10km. The rest of the days were considered as cloudy days. During the campaign, these cloudy days were observed in 41 days, which accounted for ~ 59% of total days, so they were the most frequent type of weather condition. Afterward, the hazy days were the second most common weather type during the campaign which were 20 days and made up for ~ 29% in total. Then foggy and clear days accounted for ~ 11% and ~ 1% respectively.

As indicated in Figure 3(f), the daily RH values were very high (~ 90%) on both hazy and foggy days. In fact, one of the parameters distinguishing these two types of day is the $PM_{2.5}$ concentration: The hazy days are characterized by higher daily-average $PM_{2.5}$ concentrations (75.8 ± 23.1 μg m^{-3})

compared to foggy days, for which $PM_{2.5}$ concentrations were 33.4 ± 9.5 μg m^{-3}. Moreover, the 4 pollution events (P1-P4) are all associated with hazy days. This is explained by the fog's ability to wash out the atmosphere and thus reduce air pollution. In the clear days, which appeared only one day during the campaign, daily $PM_{2.5}$ concentrations were 19.1 μg m^{-3}, while $PM_{2.5}$ concentrations in cloudy days were 32.6 ± 12.6 μg m^{-3}. The daily-average $PM_{2.5}$ concentrations can be also controlled by WS measured at 100m a.g.l.: clear days are characterized by high daily WS (5.6 m s^{-1}), while hazy days were related to lower WS (2.5 ± 0.5 m s^{-1}). WS on cloudy and foggy days were 4.1 ± 0.8 m s^{-1} and 3.3 ± 0.6 m s^{-1}, respectively. In conclusion, a strong wind, which is favorable to the dispersion of pollutants, generally induces lower concentrations of pollutants than a weak wind. Figure 3(c) indicates that there was a significant difference between WS recorded at 50m a.g.l. by the weather station and the Doppler Lidar observations at 280m. This could be explained by the complex structure of vertical wind motion and the atmospheric dynamics which are not easy to be fully monitored by meteorological ground-based devices. Thus, in order to clearly understand the role of the atmospheric dynamics on the sudden change of $PM_{2.5}$, the vertical wind speeds need to be studied in further by using the Doppler Lidar, which will be explored with the BLH in section 3.3.

The occurrence of cold surges in winter can also be a factor affecting $PM_{2.5}$ concentrations in Hanoi. During our campaign, there were 5 cold surges marked with red triangles on the time axis in Figure 3. The beginning of these cold surges was detected by (1) a significantly daily temperature drop of more than 2°C along with (2) high wind coming from the NE. For example, a first cold surge occurred in Hanoi from 14 to 17 January: the WD shifted from SE to NE (Fig. 3d), with a dramatically increased of the WS and the temperature significantly dropped. After that, the 2nd, 3rd, 4th and 5th surges were recorded on 21/01, 21/02, 05/03 and 14/03 respectively. Figure 3(f) shows the arrival of a cold surge generally coincides with a sudden drop in $PM_{2.5}$ concentrations, followed by a gradual increase in the following days when the temperature rises again. However, this decrease is not always of the same magnitude, levels of $PM_{2.5}$ clearly decrease at the arrival of the first two and the last cold surges of the campaign, but not really for the 3rd and the 4th cold surges. Thus, meteorological parameters associated with cold surges cannot predict completely the variability in $PM_{2.5}$ levels. In more general terms, conventional meteorological parameters recorded on the ground such as T, RH, WS and WD influence pollution levels, but they do not seem to be the only determining parameters. It is in fact necessary to take into account other factors to better understand the pollution events, such as the origin of air masses notably described by backward trajectory data or the structure of the boundary layer.

3.2 Local against Long-Range Transport

The results of the HYSPLIT cluster analysis over the whole campaign are presented on Figure 4 to further analyze the impact of LRT. During the scope of this study, pollution is considered from LRT when the sources are located more than 50km from the OS1. The back-trajectories of air masses arriving at 100m a.g.l. at Hanoi are classified among six clusters (Fig. 4a). For four clusters out of the six (from clusters #1a to #4a), accounting for a total of 75% of time, the air masses arrived in Hanoi by the Southeast while staying at low altitudes (i.e. inside the BL). Evidently, most of these air masses passed through the northeastern coast of Vietnam (i.e. Quang Ninh, Hai Phong, etc.) and Red River Delta (Fig. 1a) which were reported to have high number of pollution sources (Huy and Kim Oanh, 2017). Thermal power plants and industrial activities (i.e. mineral products, brick manufacturing and cement factories) are notably significant PM sources located in these areas. Thus, the air quality in several cities in these regions are highly impacted by local emissions, as demonstrated by the increase of Pb-PM_{10} in Hai Phong under NE monsoon (Chifflet et al., 2018) or $PM_{2.5}$ in Quang Ninh in winter (Hang and Kim Oanh, 2014). In this latter case, $PM_{2.5}$ was composed of organic matter, water soluble inorganic ions (NH_4^+, SO_4^{2-}, and NO_3^-), soot and crustal elements which were essentially attributed to pollution sources such as biomass burning, or to the formation of secondary inorganic aerosols. As a result, these regional sources of pollution can contaminate the air masses arriving in Hanoi and this LRT explains high PM concentrations. In addition, before reaching Vietnam, the air masses for clusters #2 and #4 flew over eastern China where $PM_{2.5}$ emissions are very high, especially on winter haze days, as observed by many studies (Ding et al., 2019; Zhang et al., 2020). The major pollutions transported from these regions include secondary sulfate-rich compounds originating from automobiles, coal-fired power stations and industrial emissions (Cohen et al., 2010b; Hai and Kim Oanh, 2013) and occasionally dust from deserts located a little more to the north (Cohen et al., 2010a). By using the chemical transport model NAAPS (from the US Naval Research Laboratory), the simulated mean of total optical depth over East Asia for the most polluted day of each pollution event (P1-P4) confirms the presence of these polluted areas in China (Figure A.2).

The mean $PM_{2.5}$ levels associated with each of these six air mass clusters is highly variable (Fig. 4a). The highest $PM_{2.5}$ concentrations were observed when the back-trajectories ending at 100m belonged to clusters #2a ($59.6 \pm 34.3 \mu g\ m^{-3}$ in average) and #4a ($48.5 \pm 29.1 \mu g\ m^{-3}$ in average), as these air masses likely accumulated pollution from eastern China and northeastern Vietnam. This situation represented a total of 36% of time during the campaign. Lower $PM_{2.5}$ concentrations were

observed when the air mass back-trajectories belonged to clusters #1a (38.1 ± 23.1 μg m^{-3} in average) and #3a (32.9 ± 12.4 μg m^{-3} in average) which flew over the sea before reaching in Hanoi, with local and Northeastern Vietnam's emissions predominantly contributing to these levels. This situation represented a total of 40% of time during the campaign. Cluster #5a (21% of time) corresponded to air masses coming at low altitude from the North, i.e. from inland China, an area that is less populated and industrialized than the eastern coast, but still has large sources of pollution (the trajectory points towards the Chongqing and Chengdu large agglomerations), thus leading to an intermediate $PM_{2.5}$ concentrations (41.3 ± 34.8 μg m^{-3} in average). Besides the dominated northeastern air masses during this time, the westerly trajectories of cluster #6a rarely occurred (3% of time) and were associated with higher levels of $PM_{2.5}$ concentrations (51.2 ± 27.6 μg m^{-3} in average). They flew over Laos and northern Thailand, a forested area in which many burning spots were visible on MODIS thermal anomaly images during the period of the campaign, especially in March (Fig. A.3). The altitude of these trajectories is high, but still compatible with catching emissions from the ground, especially smoke from large forest fires that rises in altitude due to the heat. For the back-trajectories arriving in Hanoi at 600m, 1000m and 1500m a.g.l. (Fig. 4b, c and d respectively), HYSPLIT returned five clusters similar to those found for an arriving height of 100m, only the cluster from inland China (cluster #5a) did not exist for air masses arriving at high altitude (600m and higher). The fraction of the westerly back-trajectories increased with altitude, representing 13% of time in total at 600m a.g.l. (clusters #3b and #4b) against only 3% at 100m a.g.l. (cluster #6a). This point is even more marked at higher altitudes, with 30% and 60% of westerly back-trajectories arriving at 1000m (clusters #3c and #5c) and 1500m a.g.l. (clusters #2d, #4d and #5d), respectively. Conversely, the share of the southeastern back-trajectories was maximal at an arriving height of 600m a.g.l. (87%) and then decreased as the ending altitude increased; it still accounted for 49% of the back-trajectories at 1000m a.g.l. but only for 13% at 1500m a.g.l. Thus, there is a stronger impact of the northeast monsoons at the heights of 100m and 600m than other altitudes. In the next parts, the relation of these air masses and the pollution near the ground will be further studied.

In order to highlight a possible relationship between the chemical composition of aerosols and potential source areas, the relative chemical composition of the weekly TSP samples and the origin of associated air masses ending at 100m a.g.l. are presented in Figure 5(a) and 5(b). In general, the relative contribution of sea-salt composed from Na and Cl were low (below 5% of total of TSP), although it was slightly higher for samples associated with a strong contribution from marine air

masses (clusters #1a and #3a), i.e. for samples S5, S6 and S8. In the meantime, a high contribution of minerals (Al, Si, Ca and Mg), metals (Fe, Zn) and secondary inorganic aerosols (sulfate, nitrate and ammonium) was observed during all weeks, even for sample S6 for which clean oceanic air masses were predominant. Therefore, these non seasalt aerosols have a local origin in this case, such as the Red River Delta or the northeastern coast of Vietnam. The highest $PM_{2.5}$ concentrations were observed for weekly samples S2, S3 and S9 associated with air masses dominated by continental clusters #2a, #4a and #5a, while the lowest level of $PM_{2.5}$ were observed for samples S6 and S8 associated with the domination of marine air masses from clusters #1a and #3a. Furthermore, a comparison of the TSP composition between these samples indicates a similar chemical composition although there was a huge different in TSP concentrations and origins between these weeks. This demonstrates a similarity in the major chemical composition of local particulate emissions and those coming from LRT including from other polluted regions of Vietnam and from China. This can be explained by the presence of the same types of industrial and urban sources in these geographical areas.

At last, we focused at the four major pollution events (P1 - P4) in order to understand what are the factors that explain these strong transient increases in $PM_{2.5}$. During the first episode (P1), Hanoi was dominated by a high-pressure system and below a subsidence region (Fig. A.4a). This subsidence generated a very strong temperature inversion above the BL, and the calm conditions at the surface were favorable to the accumulation of pollutants, leading to widespread haze. The levels of $PM_{2.5}$ started to increase on 18/01, when the WD shifted from strong NE winds to weaker southwest and northwest winds (Fig. 3d) and remained at high level until the arrival of a new cold surge. As expected, this one was associated with an increase in the WS and precipitation on 20/01, which put an end to this pollution event. Next, similar to the P1 event, Hanoi was also dominated by a high-pressure system during the episode P2 from 23 - 28/01 (Fig. A.4b) and the event started when the WD shifted from strong NE winds to weaker SE on 23/01. The daily $PM_{2.5}$ concentrations tended to maintain at high pollution levels until the beginning of the 28/01 with the replacement of a low-pressure system that normally brings wet and windy conditions (Fig. A.4c). Afterward, the third polluted event (P3) occurred on day 26/02 when the WD shifted from strong NE winds to weaker southwest winds along with the increase of $PM_{2.5}$ concentration. On 28/02, the appearance of low pressure system (Fig. A.4d) led to the reinforcement of WS which ended this pollution event. Finally, the last pollution event (P4) was recorded between 11 and 14 March. The $PM_{2.5}$ concentrations rose from 11/03 when the WD changed from NE to SE. Similar to the first pollution event, the arrival of a new cold surge on day 14/03 with high WS put a termination to

this event. During the first three pollution events, the air masses originating from coastal or inland China overwhelmed at lower heights, i.e. clusters #2a, #4a and #5a at 100m a.g.l. (Fig. 6a) and clusters #1b and #2b at 600m a.g.l. (Fig. 6b). For the last pollution event P4, the appearance of cluster #6a from the West (Fig. 6a) suggest an impact of transported biomass burning emission at elevated altitude. Moreover, the total optical depth from simulated-model NAAPS shows clearly the impact of smoke from biomass burning from the West on day 14/03 (P4 pollution event) (Fig. A2.d). This is consistent with scenarios in which the NE monsoon air masses pass through eastern or inland China, the northeastern regions of Vietnam and arrive in Hanoi, possibly carrying a large number of aerosols and gaseous pollutants. Consequently, LRT from the Northeast includes a combination of essentially two main polluted contributions, from the northeastern coast of Vietnam and from eastern or inland China. In addition, the impact of biomass burning from forest burning and burning activities in Laos and Thailand in March is also observed as mentioned by other studies (Huang et al., 2013; Reid et al., 2013).

However, the results shown in figure 6 does not fit with the results in figure 2, according to which steady winds from the NE to SE were associated with very low $PM_{2.5}$ levels. This means that the local WD measured by the Lidar was not always in agreement with the air mass origin, i.e. to the large-scale WD data used by HYSPLIT to compute the back-trajectories. For instance, the WD on 18/01 and 19/01 (Fig. 3d) was southwest and northwest respectively while the direction of the dominant clusters on these days was NE (cluster #5a) and SE (clusters #2a and #4a). This difference could be explained by external local factors such as lake-breeze or topography which lead to a sudden change in the local wind. As a result, models like HYSPLIT are likely more effective than local wind data in studying the LRT.

3.3 Role of the boundary layer dynamics on $PM_{2.5}$ levels during pollution events

In general, the evolution of the BL during a day can be described as follows: After the sunrise (recorded at 07:00 LT), the convective boundary layer (CBL) grows steadily and often reaches its maximum height from 14:00 to 16:00 LT. Afterward, the sensible solar radiation decreases and the CBL gradually changes into neutral boundary layer (NBL) that has a short-lived state. Around the sunset (recorded at 18:00 LT), the bottom part of the NBL is transformed into stable boundary layer (SBL) driven by weaker and sporadic turbulence under stable conditions (Stull, 1988). However, the BLH development is strongly impeded under haze conditions because a large part of the incoming solar radiation is either absorbed or scattered by the fog, by clouds or by the pollution layer, thus reducing the solar flux reaching the surface and leading to increased stability (Quan et al., 2013; Leng et al., 2016).

Lower BLH on hazy days weakens the vertical mixing and directly results in the accumulation of aerosol at the surface, leading to an increase in aerosol concentration.

Figure 3(f) shows that the daily maximum of the hourly BLH ranged from 700m to 1200m during cloudy days, depending on cloud properties (type, thickness and altitude), while it was typically below 1000m during hazy days or foggy days. Unfortunately, there are less days with maximum BLH on figure 3(f) than days with data availability in Table S1; this is because it was not always possible to retrieve the BLH due to the low-altitude clouds and precipitation. Furthermore, it is clear that the daily concentration of $PM_{2.5}$ is higher throughout a day when the maximum BLH is lower. For example, during the event P2, a sudden drop of the maximum BLH occurred from day 24 to 25/01, leading to a dramatic increase of daily $PM_{2.5}$ level on day 25/01 (Fig. 3f). Figure 7 shows the time series of BLH measured by the SLIM in Hanoi on 19/01, 24/01, 28/02 and 14/03, which corresponds to the most polluted day of each pollution event (P1-P4). High back-scattering coefficient values were recorded at altitudes lower than the BLH suggesting that the haze pollution was formed and evolved within the BL. Thus, a fine analysis of the relation between the BLH and $PM_{2.5}$ variations will be performed for these four pollution events.

3.3.1 Pollution event P1: 18 - 20/01

The analysis of the most polluted day of event P1 (19/01) indicates that the CBL grew constantly after sunrise (around 07:00 LT) when the incoming solar radiation increased. The growth rate of the boundary layer was weak (≤ 50 m h^{-1}) in the morning but increased gradually in midday (~ 80 m h^{-1}) but remained moderate as medium altitude clouds were present above the BL until 16:00 LT (Fig. 8a). The maximum BLH on this day was 660m, observed at 16:00 LT before falling gradually. After the sunset, the SBL maintained at heights around 400m to 450m until the next morning and it remained capped by low-level clouds. Besides BLH, it is important to take into account the ventilation coefficient (VC), an indicator which combines the effects of the vertical and horizontal dispersion of aerosols. VC (m^2s^{-1}) is normally defined as the horizontal wind speed integrated over the whole BL depth (Iyer and Raj, 2013; Sujatha et al., 2016); here, it was estimated as the product of hourly BLH and the hourly mean wind speed (WS) at 200m a.g.l.

Regarding $PM_{2.5}$, the concentration was already high (~ 90 µg m^{-3}) at the beginning of the day which could be a consequence of the cumulative process from the day before. Besides, the vertical mixing was weak (Fig. 9a) due to the influence of a high-pressure system associated with low SBL height, enhancing the accumulation of pollutants near the surface. During the first 2 hours of the day, $PM_{2.5}$ concentrations increased to reach 106 µg m^{-3} at 02:00 LT. Afterward, the concentration of $PM_{2.5}$

fell gradually to 68 μg m^{-3} between 02:00 and 07:00 LT although there was no significant variation of BLH at that moment. This decrease could be explained by the existence of a weak low-level jet (LLJ) in very stable conditions that was recorded by the Doppler Lidar between 02:00 and 05:0 LT around 180 m altitude (Fig. 9a). The radiosonde profile recorded at 07:00 LT (Fig. A.5a) shows the presence of another weak LLJ (2 - 3 m s^{-1}) located beyond the Doppler Lidar range and just below the SBL top. These jets were able to result in a sudden increase of vertical mixing at lower levels, leading to the dispersion of pollutants near the surface (Mahrt, 2014; Wei et al., 2018).

After the sunrise, the concentration of $PM_{2.5}$ started to rise following the increase of emitting activities, such as vehicles or cooking, during the rush hours, which occurred in a still slowly growing BL. Around 16:00 LT, the $PM_{2.5}$ levels decreased slightly when the BLH reached its maximum height, before rising once again from 18:00 LT. This evening increase in PM is likely due to the combination between the depletion of BL and the second rush hour also starting from 18:00 LT. Interestingly, the $PM_{2.5}$ concentration continued to rise rapidly despite a considerable reduction of vehicle activities and others after the end of rush hour around 20:00 LT. This $PM_{2.5}$ increase was in fact associated with very weak vertical mixing as indicated by the low VC observed at this time (Fig. 9a), leading to the poor dispersion of particles and the accumulation of $PM_{2.5}$ near the surface.

3.3.2 Pollution event P2: 23 - 28/01

The analysis of 24/01 shows that the CBL also grew constantly after sunrise, along with the increase of incoming solar radiation in the morning (Fig. 7b). However, the growth rate of the CBL during daytime on 24/01 was faster (~100 m h^{-1}) than that on 19/01. The maximum height was 780m, observed at 15:00 LT. Then, the BLH collapsed suddenly with a higher decay rate compared to day 19/01. At night, this layer maintained at a stable height of approximately 300m from 22:00 LT until the next early morning.

At midnight, the $PM_{2.5}$ concentration was high (~90 μg m^{-3}) then decreased gradually (Fig. 8b) until sunrise (07:00 LT). After that, the concentration of $PM_{2.5}$ increased rapidly and reached a peak at 10:00 LT. This could be explained by enhanced transport activities in the first rush hour, associated with the low BL height in the morning. Furthermore, the wind speeds during this period were weak, with values ≤ 2 m s^{-1}, leading to low values of VC and mixing (Fig. 9b). After 10:00 LT, the $PM_{2.5}$ levels decreased, along with a rapid increase of BLH, which reached its maximum height at 15:00 LT. The increase in VC in this period may be attributed to the fact that both BLH and WS show an ascending trend, enhancing the air quality. From 16:00 LT, the $PM_{2.5}$ concentrations tended to increase

slightly once again and reached a peak at 20:00 LT. This trend was again the result of a combination of the decrease of BLH and the second rush hour after the sunset. Afterward, the $PM_{2.5}$ concentration fell gradually but still remained at a high level (~ 70 µg m^{-3}) at night due to the low height of the SBL. Contrary to the 19/01, no LLJ was visible on this day within the SBL, either on the wind Lidar observations (Fig. 9b) or on the radiosondes profiles (at 07:00 and 19:00 LT, Fig. A.5b). In general, this result is consistent with low BLH and WS measured on day 24/01.

3.3.3 Pollution event P3: 26 - 28/02

Day 28/02 was one of the rare hazy days in February, and this day was also associated with the third pollution event. After sunrise, the height of the BL started to increase with a weak growth rate ($\leq$ 50 m h^{-1}) from 07:00 to 11:00 LT (Fig. 8c). From 11:00 to 14:00 LT, the BLH increased rapidly and reached its maximum height of 850m at 14:00 LT (more than on 19/01 and 24/01). Then, the BL decayed due to the decrease of the sensible solar radiation in the late afternoon.

Concerning $PM_{2.5}$ concentration, it was high at the beginning of the day (~80 µg m^{-3}) and remained this way until 12:00 LT (Fig. 8c). This phenomenon might be due to the low height of the SBL at night and the slow growth of CBL in the morning, which weakened the mixing (Fig. 9c), leading to the accumulation of $PM_{2.5}$ near the ground. During the campaign, the BLH retrieved from 00:00 to 11:00 LT was generally lower than what was observed on 19 and 24 January, as it mainly varied in the range of 300 - 350 m. Afterward, the concentration of $PM_{2.5}$ started to fall gradually with the simultaneous increase of the BLH, which reached its maximum altitude at 15:00 LT, leading to the increase of vertical mixing near the surface (Fig. 9c). In addition, an increase of VC was also recorded at the moment. More generally, higher values of VC were observed on day 28/02 (Fig. 9c) due to the higher BLH. Then, the concentration of $PM_{2.5}$ declined more rapidly after 16:00 LT (from ~ 77 µg m^{-3} to less than 35 µg m^{-3}) due to the increase of WS under the impact of low-pressure system. Especially, LLJ located just below the SBL top (~ 400m) were recorded at 19:00 LT (Fig. A.5c). Then, these LLJ combined with the wind shear (Fig. 9c) to form intermittent turbulence at lower levels that was recorded by the Doppler Lidar during at night around 200m to 280m a.g.l, enhancing the mixing and increasing the dispersion of $PM_{2.5}$ near the surface.

3.3.4 Pollution event P4: 11 - 14/03

Day 14/03 was the last day and the most polluted day during the period P4. Concerning the boundary layer, the heights of SBL on this day was commonly higher than these on other cases (with heights $\geq$ 500m from 03:00 to 07:00 LT). Furthermore, CBL evolved slowly with a rate $\leq$ 40 m h^{-1} after

the sunrise. And BLH reached the highest altitude at 890m at 14:00 LT (Fig. 8d) before decreasing over time as a normal scenario for the depletion of the CBL in the late afternoon. After 23:00 LT, the BLH could not be retrieved because of the precipitation.

At the beginning of the day, the $PM_{2.5}$ concentration was lower than during the other cases (~ 60 μg m^{-3}) but it was still considered a high concentration. This result is expected considering that this day had the highest value of VC of the four case studies (Fig. 9d). Later on, the $PM_{2.5}$ concentration suddenly increased from 03:00 LT and after two hours, it reached ~ 130 μg m^{-3} which was twice as much as its value at the beginning of the day (Fig. 8d). The Doppler Lidar shows that a LLJ probably existed from 04:00 to 09:00 LT (Fig. 9d), though the top of the jet was visible only on the radiosonde profile at 07:00 LT (Fig. A.5d). This jet could have carried pollutants from regional sources to Hanoi, leading to the increase of $PM_{2.5}$. Also, the increased wind shear below the jet reinforced the vertical mixing leading to the irruption of pollutants at the surface. Afterward, the $PM_{2.5}$ concentration went down slightly but it maintained at a high polluted level (≥ 100 μg m^{-3}) until 14:00 LT, as the boundary layer only grew moderately after sunrise. After the BLH reached its maximum height of 910m at 14:00 LT, it tended to decrease gradually and the concentration of $PM_{2.5}$ began to increase until 20:00 LT because of the depletion of the BL. Then, the concentration of $PM_{2.5}$ fell suddenly by the arrival of a new cold surge, which resulted in a significant increase in WS.

3.4 Discussion

The main goal of our study was to identify key factors explaining the pollution events during the winter season in Vietnam, by considering all phenomena that could contribute to air pollution, i.e. local meteorological parameters, vertical wind profiles, BLH, air mass trajectories… At a large geographic scale, our results indicate a significant impact of LRT on air quality during winter 2019, especially during pollution events. The increase of $PM_{2.5}$ during these events corresponds mainly to large scale pollutant transport from the Northeast, under the winter monsoon's impact, which is in agreement with previous studies (Hien et al., 2004; Hai and Kim Oanh, 2013; Ly et al., 2020). In addition, the pollution can sometimes come from high altitude LRT of biomass burning emissions from the West, as observed for the event P4. Nevertheless, the LRT of pollution alone does not explain the temporal variability of $PM_{2.5}$ levels in Hanoi. A complementary analysis of the local atmospheric dynamics is necessary.

The impact of meteorological factors (i.e. humidity, temperature) is known to influence the variation of pollutant concentrations at the surface in winter (Hien et al., 2011; Nguyen et al., 2020). However, while previous studies only considered WS and WD data from ground observations, the

hourly vertical structure of turbulence and vertical mixing profiles were measured precisely in this study, and they revealed to be determinant parameters governing the hourly variability of $PM_{2.5}$ during pollution events. The vertical mixing measured by Doppler Lidar can vary significantly with the evolution of incoming solar radiation during daytime, while it can be reinforced during nighttime when a LLJ appears. These vertical mixing evolutions could lead to the accumulation or dispersion of $PM_{2.5}$ at the surface, as observed during the four pollution events in winter 2019 (Figure 9). The approach proposed in this study brings a more accurate view for understanding the PM variations under stagnant condition in Hanoi.

In addition, the dynamics of $PM_{2.5}$ concentrations in the boundary layer is closely related to the height of this layer (Stull, 1988; Cohn and Angevine, 2000; Boyouk et al., 2010; Altstädter et al., 2018). Thus, the study of BLH here provides for the first time a complementary analysis on PM2.5 variations during pollution events, while there is still limited information on the BLH evolution in Southeast Asia, particularly in Vietnam. The maximum BLH in Hanoi ranges from 700m to 1200m with values systematically below 1000m during hazy days. Besides, having simultaneous measurements of the wind profile and BLH allows to determine the ventilation coefficient, a synthetic parameter characterizing the pollutant dispersion which is of high interest for air pollution monitoring and assessment. The high hourly $PM_{2.5}$ concentration during hazy days is essentially consistent with the slower growth of BLH and lower ventilation coefficient. Consequently, this analysis suggests that BLH is an essential parameter to understand the mechanism connecting atmospheric dynamic factors and air quality in Hanoi during the winter period.

4. Summary

To identify the factors affecting air pollution, this study analyzed the relationship between multi-scale meteorological conditions and pollution events during the winter 2019. The mean $PM_{2.5}$ concentration during the campaign that took place in Hanoi from 11/01 to 22/03/2019 was 45 ± 25 $\mu g.m^{-3}$. The highest daily level of $PM_{2.5}$ was recorded on 25/01 (129 $\mu g\ m^{-3}$), while lower levels of $PM_{2.5}$ were mainly observed in February.

Four severely pollution events were recorded during the campaign, associated with stagnant conditions. The results of HYSPLIT backward trajectories showed that the three first pollution events were mainly related to the occurrence of LRT from China and from the northeast coastal regions of Vietnam. In addition, a mix of two LRT contributions was recorded during the fourth pollution event, that included emissions from the Northeast and biomass burning from the West. However, the chemical

composition of TSP was pretty constant over the 10 weeks of sampling, which included both periods associated with LRT aerosols and other periods with only local emissions. This indicates that locally emitted particles had a major chemical composition which was relatively similar to those coming from LRT.

Besides, the aerosol Lidar observations showed a large variability in the daytime BLH according to the different weather conditions: the daily maximum of the hourly BLH varied from 700m up to 1200m during cloudy days, while it was typically below 1000m during hazy days. In hazy days, the height of the boundary layer was compressed and grew slowly within just a few hundred meters due to the strong effect of haze. Because of the lower BLH, the accumulation of pollutants at the surface was reinforced, leading to severe degradations of the air quality in Hanoi.

Our study provides a better understanding of the mechanisms linking meteorological parameters, BLH and air quality during the winter period in Hanoi. The methods and results presented here can be used to further assess the contents, types and controlling factors of atmospheric dynamics on polluted events in Hanoi under different weather conditions and season, or in other cities in South-East Asia.

Acknowledgments

The authors sincerely acknowledge the financial support from the Institute Environmental Technology funded by Vietnam National Independent (Science & Technology) Program for Space Technology (CNVT/16-20) under the grant number VT-UD.11/17-20. This work is a contribution to the CPER (Contrat de Plan Etat-Région) research project IRenE (Innovation et Recherche en Environnement) and Climibio. The work is supported by the French Ministère de l'Enseignement Supérieur, de la Recherche et de l'Innovation, the region Hauts-de-France and the European Regional Development Fund. The work is also supported by the CaPPA project. The CaPPA project (Chemical and Physical Properties of the Atmosphere) is funded by the French National Research Agency (ANR) through the PIA (Programme d'Investissement d'Avenir; contract no. ANR-11-LABX-0005-01) and by the regional council of Nord-Pas-de-Calais and the European Regional Development Fund.

We appreciate LPCA, Université du Littoral Côte d'Opale for providing the Doppler Lidar (Windcube V2) and LATMOS, CNRS & Paris Sorbonne University for providing the aerosol micro-pulse Lidar (SLIM). The regional online databases of pollutants and meteorology provided by different websites are genuinely appreciated, especially the $PM_{2.5}$ database from Environmental Protection Agency (EPA) and radiosonde data from the Department of Atmospheric Science of Wyoming

592 University. The few anonymous people who provided information in the context of a personal
593 relationship are sincerely acknowledged for their valuable contributions.

594 ***Author Contributions:** All authors contributed significantly to this manuscript. Phung Ngoc Bao
595 Anh wrote the manuscript draft with contributions from Hervé Delbarre, Karine Deboudt and Elsa
596 Dieudonné. All authors participated to the field campaign. Nguyen Tran Dien and Le Thanh Son
597 funded to the transport of equipment for the field campaign. Hervé Delbarre, Karine Deboudt, Elsa
598 Dieudonné and Phung Ngoc Bao Anh performed and monitored the experiments. Hervé Delbarre
599 directed the experiments. Jacques Pelon and François Ravetta revised the manuscript draft and
600 provided valuable suggestions for the revision.

601 ## References

Altstädter, B., Platis, A., Jähn, M., Baars, H., Lückerath, J., Held, A., Lampert, A., Bange, J., Hermann, M., Wehner, B., 2018. Airborne observations of newly formed boundary layer aerosolparticles under cloudy conditions (preprint). Aerosols/Field Measurements/Troposphere/Physics (physical properties and processes). https://doi.org/10.5194/acp-2017-1133

Boyouk, N., Léon, J.-F., Delbarre, H., Podvin, T., Deroo, C., 2010. Impact of the mixing boundary layer on the relationship between PM2.5 and aerosol optical thickness. Atmos. Environ. 44, 271–277. https://doi.org/10.1016/j.atmosenv.2009.06.053

Cabello, M., Orza, J.A.G., Galiano, V., Ruiz, G., 2008. Influence of meteorological input data on backtrajectory cluster analysis - a seven year study for southeastern Spain. Adv. Sci. Res. 2, 65–70. https://doi.org/10.5194/asr-2-65-2008

Chifflet, S., Amouroux, D., Bérail, S., Barre, J., Van, T.C., Baltrons, O., Brune, J., Dufour, A., Guinot, B., Mari, X., 2018. Origins and discrimination between local and regional atmospheric pollution in Haiphong (Vietnam), based on metal (loid) concentrations and lead isotopic ratios in PM10. Environ. Sci. Pollut. Res. 25, 26653–26668. https://doi.org/10.1007/s11356-018-2722-7

Cohen, D.D., Crawford, J., Stelcer, E., Bac, V.T., 2010a. Long range transport of fine particle windblown soils and coal fired power station emissions into Hanoi between 2001 to 2008. Atmos. Environ. 44, 3761–3769. https://doi.org/10.1016/j.atmosenv.2010.06.047

Cohen, D.D., Crawford, J., Stelcer, E., Bac, V.T., 2010b. Characterisation and source apportionment of fine particulate sources at Hanoi from 2001 to 2008. Atmos. Environ. 44, 320–328. https://doi.org/10.1016/j.atmosenv.2009.10.037

Cohn, S.A., Angevine, W.M., 2000. Boundary Layer Height and Entrainment Zone Thickness Measured by Lidars and Wind-Profiling Radars. J. Appl. Meteorol. 39, 15. https://doi.org/10.1175/1520-0450(2000)039<1233:BLHAEZ>2.0.CO;2

Delbarre, H., Augustin, P., Saïd, F., Campistron, B., Bénech, B., Lohou, F., Puygrenier, V., Moppert, C., Cousin, F., Fréville, P., Fréjafon, E., 2005. Ground-based remote sensing observation of the complex behaviour of the Marseille boundary layer during ESCOMPTE. Atmospheric Res. 74, 403–433. https://doi.org/10.1016/j.atmosres.2004.04.007

Dieudonné, E., Chazette, P., Marnas, F., Totems, J., Shang, X., 2017. Raman Lidar Observations of Aerosol Optical Properties in 11 Cities from France to Siberia. Remote Sens. 9, 978. https://doi.org/10.3390/rs9100978

Ding, A., Huang, X., Nie, W., Chi, X., Xu, Zheng, Zheng, L., Xu, Zhengning, Xie, Y., Qi, X., Shen, Y., Sun, P., Wang, J., Wang, L., Sun, J., Yang, X.-Q., Qin, W., Zhang, X., Cheng, W., Liu, W., Fu, C., 2019. Significant reduction of PM 2.5 in eastern China due to regional-scale emission control: evidence from SORPES in 2011–2018. Atmospheric Chem. Phys. 19, 11791–11801. https://doi.org/10.5194/acp-19-11791-2019

Draxler, R.R., Hess, G.D., 1998. An Overview of the HYSPLIT_4 Modelling System for Trajectories, Dispersion, and Deposition. Aust. Meteorol. Mag. 47, 295–308.

Flamant, C., Pelon, J., Flamant, P.H., Durand, P., 1997. Lidar determination of the entrainment zone thickness at the top of the unstable marine atmospheric boundary layer. Bound.-Layer Meteorol. 83, 247–284. https://doi.org/10.1023/A:1000258318944

Hai, B.V., Tuan, N.X., Hoang, N.D., Trung, D.V., 2013. Monitoring the boundary layer over Hanoi using a compact Lidar system with a high power diode laser at 905 nm. Presented at the Proc. of the 2nd Academic Conference on Natural Science for Master and PhD Students from Cambodia – Laos – Malaysia – Vietnam, p. 9.

Hai, C.D., Kim Oanh, N.T., 2013. Effects of local, regional meteorology and emission sources on mass and compositions of particulate matter in Hanoi. Atmos. Environ. 78, 105–112. https://doi.org/10.1016/j.atmosenv.2012.05.006

Hang, N.T., Kim Oanh, N.T., 2014. Chemical characterization and sources apportionment of fine particulate pollution in a mining town of Vietnam. Atmospheric Res. 145–146, 214–225. https://doi.org/10.1016/j.atmosres.2014.04.009

Hennemuth, B., Lammert, A., 2006. Determination of the Atmospheric Boundary Layer Height from Radiosonde and Lidar Backscatter. Bound.-Layer Meteorol. 120, 181–200. https://doi.org/10.1007/s10546-005-9035-3

Hien, P.D., Bac, V.T., Thinh, N.T.H., 2004. PMF receptor modelling of fine and coarse PM10 in air masses governing monsoon conditions in Hanoi, northern Vietnam. Atmos. Environ. 38, 189–201. https://doi.org/10.1016/j.atmosenv.2003.09.064

Hien, P.D., Loc, P.D., Dao, N.V., 2011. Air pollution episodes associated with East Asian winter monsoons. Sci. Total Environ. 409, 5063–5068. https://doi.org/10.1016/j.scitotenv.2011.08.049

Huang, K., Fu, J.S., Hsu, N.C., Gao, Y., Dong, X., Tsay, S.-C., Lam, Y.F., 2013. Impact assessment of biomass burning on air quality in Southeast and East Asia during BASE-ASIA. Atmos. Environ. 78, 291–302. https://doi.org/10.1016/j.atmosenv.2012.03.048

Huy, L.N., Kim Oanh, N.T., 2017. Assessment of national emissions of air pollutants and climate forcers from thermal power plants and industrial activities in Vietnam. Atmospheric Pollut. Res. 8, 503–513. https://doi.org/10.1016/j.apr.2016.12.007

Iyer, U.S., Raj, P.E., 2013. Ventilation coefficient trends in the recent decades over four major Indian metropolitan cities. J. Earth Syst. Sci. 122, 537–549. https://doi.org/10.1007/s12040-013-0270-6

Janta, R., Sekiguchi, K., Yamaguchi, R., Sopajaree, K., Pongpiachan, S., Chetiyanukornkul, T., 2020. Ambient PM2.5, polycyclic aromatic hydrocarbons and biomass burning tracer in Mae Sot District, western Thailand. Atmospheric Pollut. Res. 11, 27–39. https://doi.org/10.1016/j.apr.2019.09.003

Kelly, F.J., Fussell, J.C., 2012. Size, source and chemical composition as determinants of toxicity attributable to ambient particulate matter. Atmos. Environ. 60, 504–526. https://doi.org/10.1016/j.atmosenv.2012.06.039

Koscielny, A.J., Doviak, R.J., Zrnic, D.S., 1984. An Evaluation of the Accuracy of Some Radar Wind Profiling Techniques. J. Atmospheric Ocean. Technol. 1, 309–320. https://doi.org/10.1175/1520-0426(1984)001<0309:AEOTAO>2.0.CO;2

Lasko, K., Vadrevu, K.P., Nguyen, T.T.N., 2018. Analysis of air pollution over Hanoi, Vietnam using multi-satellite and MERRA reanalysis datasets. PLOS ONE 13, e0196629. https://doi.org/10.1371/journal.pone.0196629

Leng, C., Duan, J., Xu, C., Zhang, H., Wang, Yifan, Wang, Yanyu, Li, X., Kong, L., Tao, J., Zhang, R., Cheng, T., Zha, S., Yu, X., 2016. Insights into a historic severe haze event in Shanghai: synoptic situation,boundary layer and pollutants. Atmospheric Chem. Phys. 16, 9221–9234. https://doi.org/10.5194/acp-16-9221-2016

Liu, B., Ma, Y., Gong, W., Zhang, M., Shi, Y., 2019. The relationship between black carbon and atmospheric boundary layer height. Atmospheric Pollut. Res. 10, 65–72. https://doi.org/10.1016/j.apr.2018.06.007

Ly, B.-T., Matsumi, Y., Nakayama, T., Sakamoto, Y., Kajii, Y., Nghiem, T.-D., 2018. Characterizing PM2.5 in Hanoi with New High Temporal Resolution Sensor. Aerosol Air Qual. Res. 18, 2487–2497. https://doi.org/10.4209/aaqr.2017.10.0435

Ly, B.-T., Matsumi, Y., Vu, T.V., Sekiguchi, K., Nguyen, T.-T., Pham, C.-T., Nghiem, T.-D., Ngo, I.-H., Kurotsuchi, Y., Nguyen, T.-H., Nakayama, T., 2020. The effects of meteorological conditions and long-range transport on PM2.5 levels in Hanoi revealed from multi-site measurement using compact sensors and machine learning approach. J. Aerosol Sci. 105716. https://doi.org/10.1016/j.jaerosci.2020.105716

Mahrt, L., 2014. Stably Stratified Atmospheric Boundary Layers. Annu. Rev. Fluid Mech. 46, 23–45. https://doi.org/10.1146/annurev-fluid-010313-141354

Marris, H., Deboudt, K., Augustin, P., Flament, P., Blond, F., Fiani, E., Fourmentin, M., Delbarre, H., 2012. Fast changes in chemical composition and size distribution of fine particles during the near-field transport of industrial plumes. Sci. Total Environ. 427–428, 126–138. https://doi.org/10.1016/j.scitotenv.2012.03.068

Menut, L., Flamant, C., Pelon, J., Flamant, P.H., 1999. Urban boundary-layer height determination from lidar measurements over the Paris area. Appl. Opt. 38, 945. https://doi.org/10.1364/AO.38.000945

MONRE, 2013. Ministry of Natural Resources and Environment. National State of Environment: Air Environment; Vietnam Publishing House of Natural Resources, Environment and Cartography: Hanoi, Vietnam.

MONRE, 2007. Ministry of Natural Resources and Environment. National State of Environment: Vietnam urban air environment, National state of Environment 2007.

Nguyen, G.T.H., Shimadera, H., Uranishi, K., Matsuo, T., Kondo, A., 2019. Numerical assessment of PM2.5 and O3 air quality in Continental Southeast Asia: Impacts of potential future climate change. Atmos. Environ. 215, 116901. https://doi.org/10.1016/j.atmosenv.2019.116901

Nguyen, T.H., Nagashima, T., Doan, Q.-V., 2020. Air Quality Modeling Study on the Controlling Factors of Fine Particulate Matter (PM2.5) in Hanoi: A Case Study in December 2010. Atmosphere 11, 733. https://doi.org/10.3390/atmos11070733

Pan, L., Xu, J., Tie, X., Mao, X., Gao, W., Chang, L., 2019. Long-term measurements of planetary boundary layer height and interactions with PM2.5 in Shanghai, China. Atmospheric Pollut. Res. 10, 989–996. https://doi.org/10.1016/j.apr.2019.01.007

Pope, C.A., Coleman, N., Pond, Z.A., Burnett, R.T., 2020. Fine particulate air pollution and human mortality: 25+ years of cohort studies. Environ. Res. 183, 108924. https://doi.org/10.1016/j.envres.2019.108924

Quan, J., Gao, Y., Zhang, Q., Tie, X., Cao, J., Han, S., Meng, J., Chen, P., Zhao, D., 2013. Evolution of planetary boundary layer under different weather conditions, and its impact on aerosol concentrations. Particuology 11, 34–40. https://doi.org/10.1016/j.partic.2012.04.005

Reddington, C.L., Conibear, L., Knote, C., Silver, B.J., Arnold, S.R., Spracklen, D.V., 2019. Exploring the impacts of anthropogenic emission sectors on PM2.5 and human health in South and East Asia. Aerosols/Atmospheric Modelling/Troposphere/Physics (physical properties and processes). https://doi.org/10.5194/acp-2019-147

Reid, J.S., Hyer, E.J., Johnson, R.S., Holben, B.N., Yokelson, R.J., Zhang, J., Campbell, J.R., Christopher, S.A., Di Girolamo, L., Giglio, L., Holz, R.E., Kearney, C., Miettinen, J., Reid, E.A., Turk, F.J., Wang, J., Xian, P., Zhao, G., Balasubramanian, R., Chew, B.N., Janjai, S., Lagrosas, N., Lestari, P., Lin, N.-H., Mahmud, M., Nguyen, A.X., Norris, B., Oanh, N.T.K., Oo, M., Salinas, S.V., Welton, E.J., Liew, S.C., 2013. Observing and understanding the Southeast Asian aerosol system by remote sensing: An initial review and analysis for the Seven Southeast Asian Studies (7SEAS) program. Atmospheric Res. 122, 403–468. https://doi.org/10.1016/j.atmosres.2012.06.005

Seinfeld, J.H., Pandis, S.N., 2006. Atmospheric Chemistry and Physics: From Air Pollution to Climate Change, 2nd Edition. ed. Wiley-Interscience, Hoboken, N.J.

Stohl, A., 1998. Computation, accuracy and applications of trajectories - A review and bibliography. Atmos. Environ. 32, 947–966. https://doi.org/10.1016/S1352-2310(97)00457-3

Stull, R.B. (Ed.), 1988. An Introduction to Boundary Layer Meteorology. Springer Netherlands, Dordrecht. https://doi.org/10.1007/978-94-009-3027-8

Sujatha, P., Mahalakshmi, D.V., Ramiz, A., Rao, P.V.N., Naidu, C.V., 2016. Ventilation coefficient and boundary layer height impact on urban air quality. Cogent Environ. Sci. 2, 1125284. https://doi.org/10.1080/23311843.2015.1125284

Tang, I.N., Munkelwitz, H.R., 1994. Aerosol Phase Transformation and Growth in the Atmosphere. J. Appl. Meteorol. 1988-2005 33, 791–796.

Taylor, D., 2010. Biomass burning, humans and climate change in Southeast Asia. Biodivers. Conserv. 19, 1025–1042. https://doi.org/10.1007/s10531-009-9756-6

Wei, W., Zhang, H., Wu, B., Huang, Y., Cai, X., Song, Y., Li, J., 2018. Intermittent turbulence contributes to vertical dispersion of $PM_{2.5}$ in the North China Plain: cases from Tianjin. Atmospheric Chem. Phys. 18, 12953–12967. https://doi.org/10.5194/acp-18-12953-2018

Yang, T., Wang, Z., Zhang, W., Gbaguidi, A., Sugimoto, N., Wang, X., Matsui, I., Sun, Y., 2017. Technical note: Boundary layer height determination from lidar for improving air pollution episode modeling: development of new algorithm and evaluation. Atmospheric Chem. Phys. 17, 6215–6225. https://doi.org/10.5194/acp-17-6215-2017

Zhang, W., Wang, H., Zhang, X., Peng, Y., Zhong, J., Wang, Y., Zhao, Y., 2020. Evaluating the contributions of changed meteorological conditions and emission to substantial reductions of PM2.5 concentration from winter 2016 to 2017 in Central and Eastern China. Sci. Total Environ. 716, 136892. https://doi.org/10.1016/j.scitotenv.2020.136892Altstädter, B., Platis, A., Jähn, M., Baars, H., Lückerath, J., Held, A., Lampert, A., Bange, J., Hermann, M., Wehner, B., 2018. Airborne observations of newly formed boundary layer aerosolparticles under cloudy conditions (preprint). Aerosols/Field Measurements/Troposphere/Physics (physical properties and processes). https://doi.org/10.5194/acp-2017-1133

FIGURES:

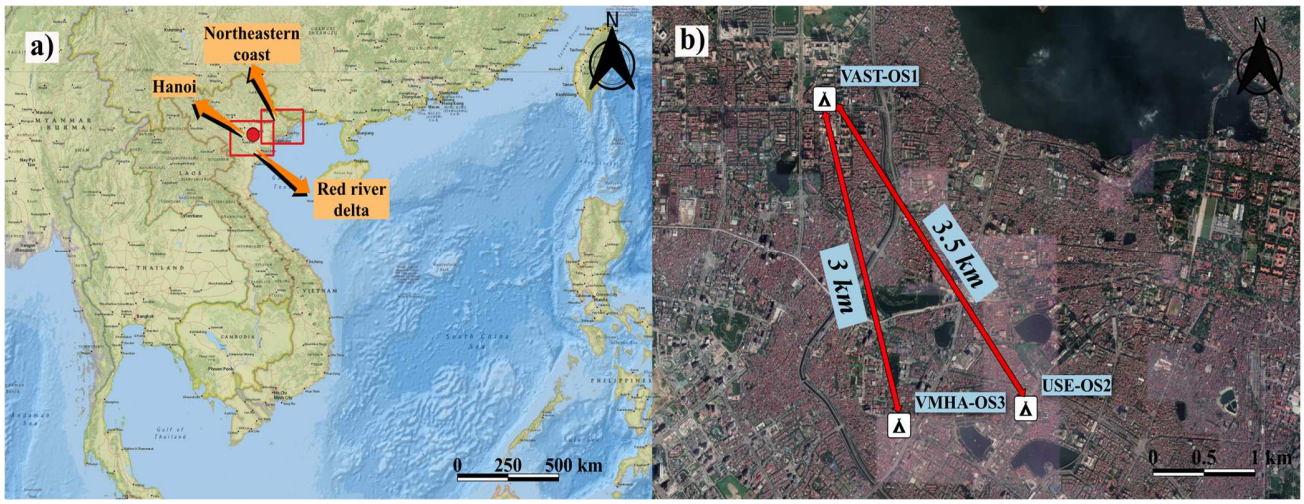

Figure 1: (a) Location of Hanoi, Red River Delta and northeastern coast of Vietnam and (b) three observation sites (VAST - OS1), (USE - OS2) and (VMHA - OS3).

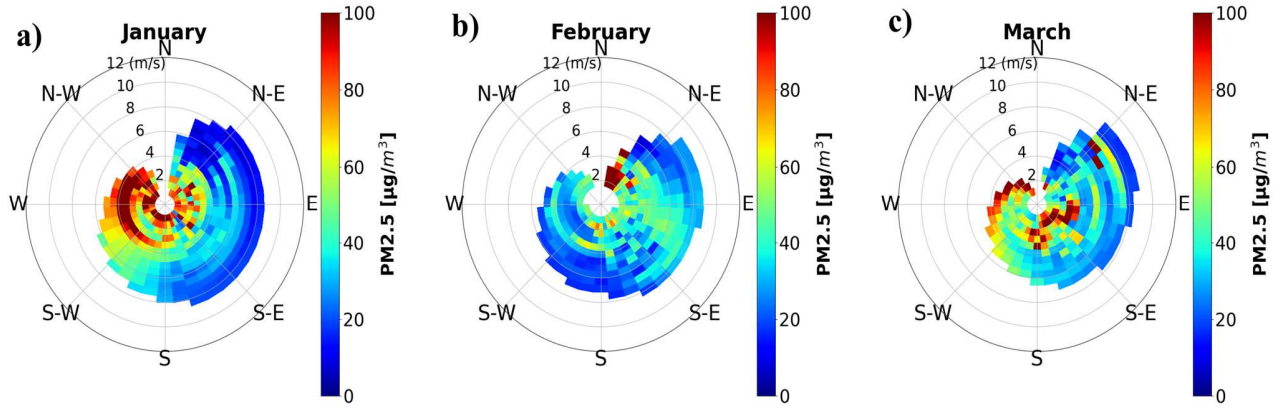

Figure 2: Bivariate polar plots of $PM_{2.5}$ concentrations at site VAST - OS1 for each month. The radial and tangential axes represent the wind direction and speed in m s^{-1} at 100m a.g.l.

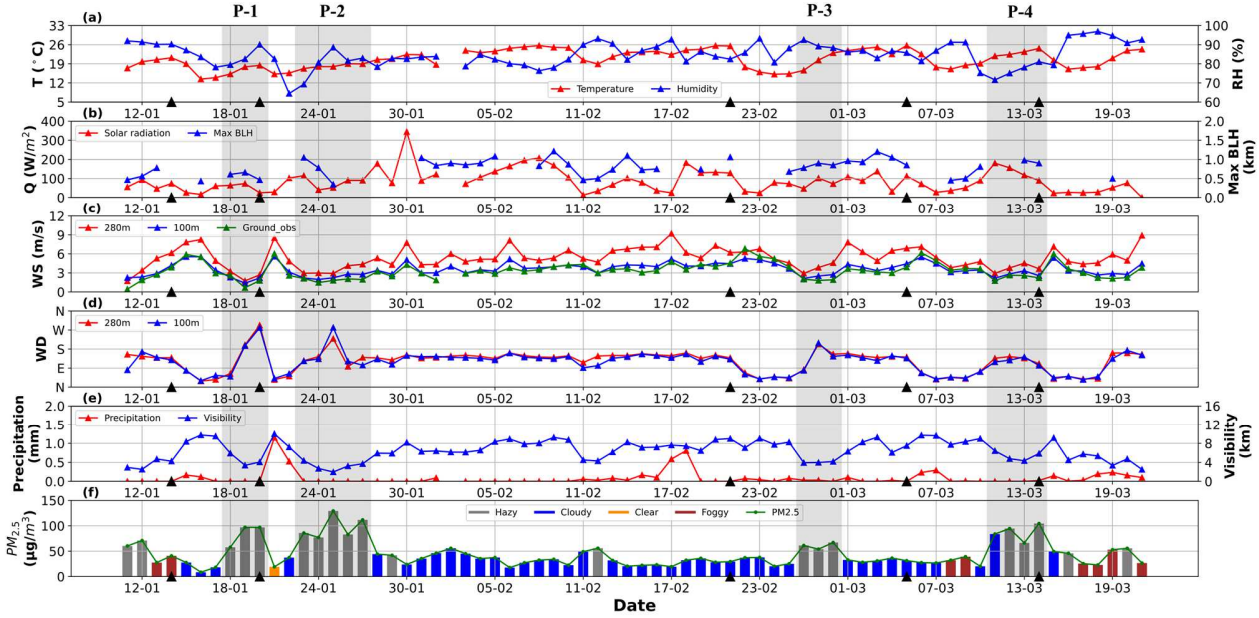

Figure 3: The daily average (a) air temperature (T) and humidity (RH), (b) Solar radiation (Q) and the daily maximum of the hourly BLH values (max BLH), (c) wind speeds (WS) at 100m, 280m a.g.l. and ground-based, (d) wind direction (WD) at 100m and 280m a.g.l., (e) precipitation and visibility, (f) $PM_{2.5}$ concentrations. Black triangles on the horizontal axis mark the cold surges. P1 - P4 represent polluted events as grey areas.

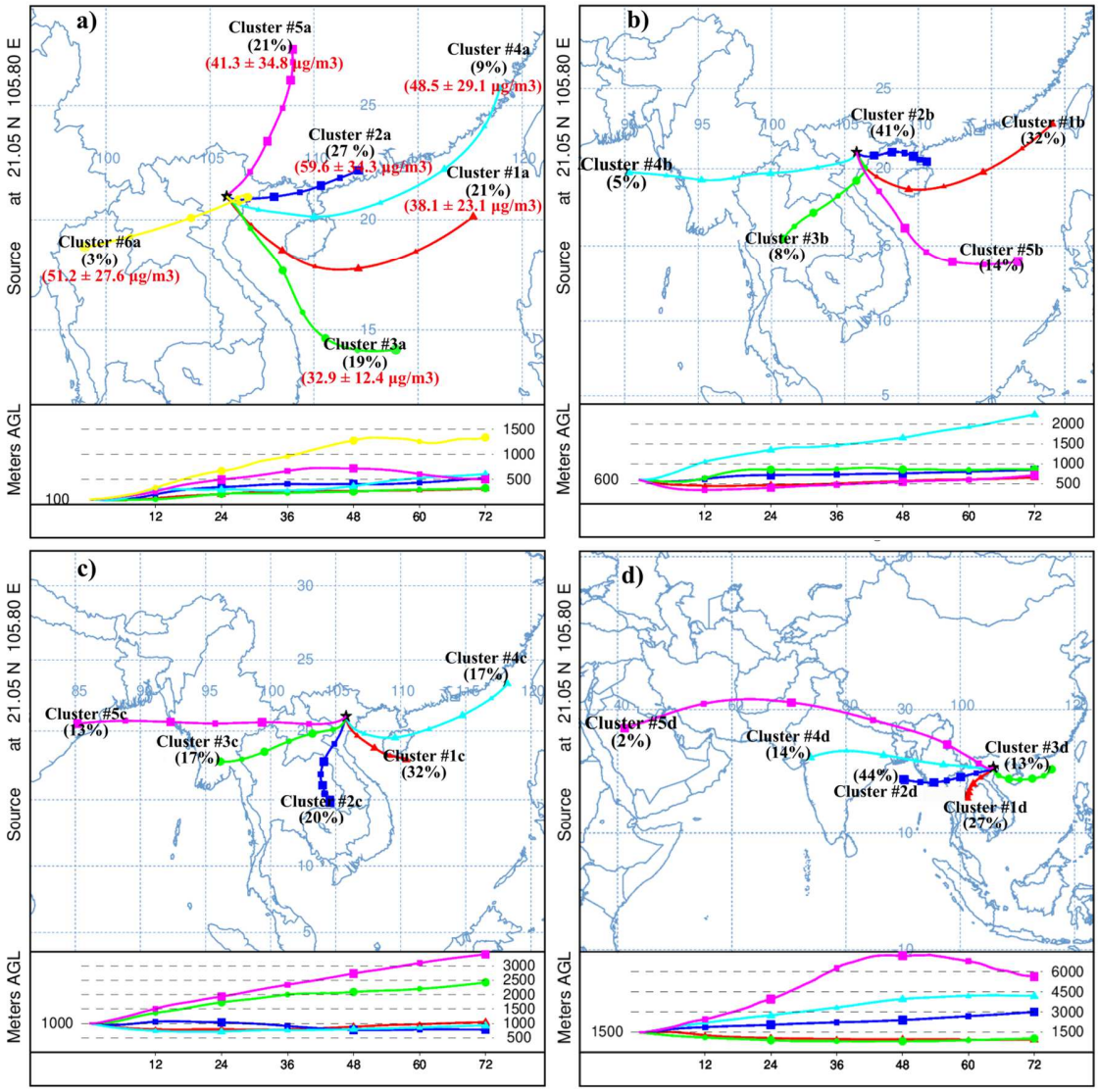

Figure 4: Cluster of HYSPLIT 72-hour back-trajectories arriving in Hanoi at heights of (a) 100 m, (b) 600 m, (c) 1000 m and (d) 1500 m a.g.l. from 11/01 to 21/03/2019.

Statistical summary of frequency and $PM_{2.5}$ concentration (mean ± one standard deviation) as a function of clusters of air masses arriving in Hanoi ending at 100m a.g.l.

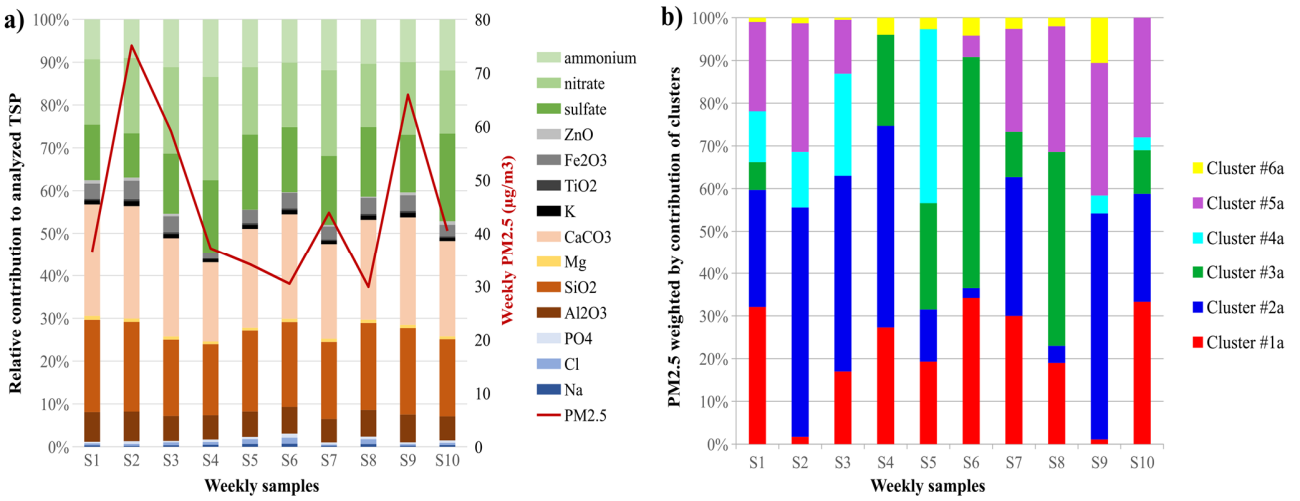

Figure 5: a) Relative chemical composition of the Total Suspended Particles (TSP) associated to the weekly samples collected at site OS1, along with the corresponding $PM_{2.5}$ concentrations ; b) relative contribution of the HYSPLIT clusters for back-trajectories ending at 100m a.g.l. in the ten weekly samples.

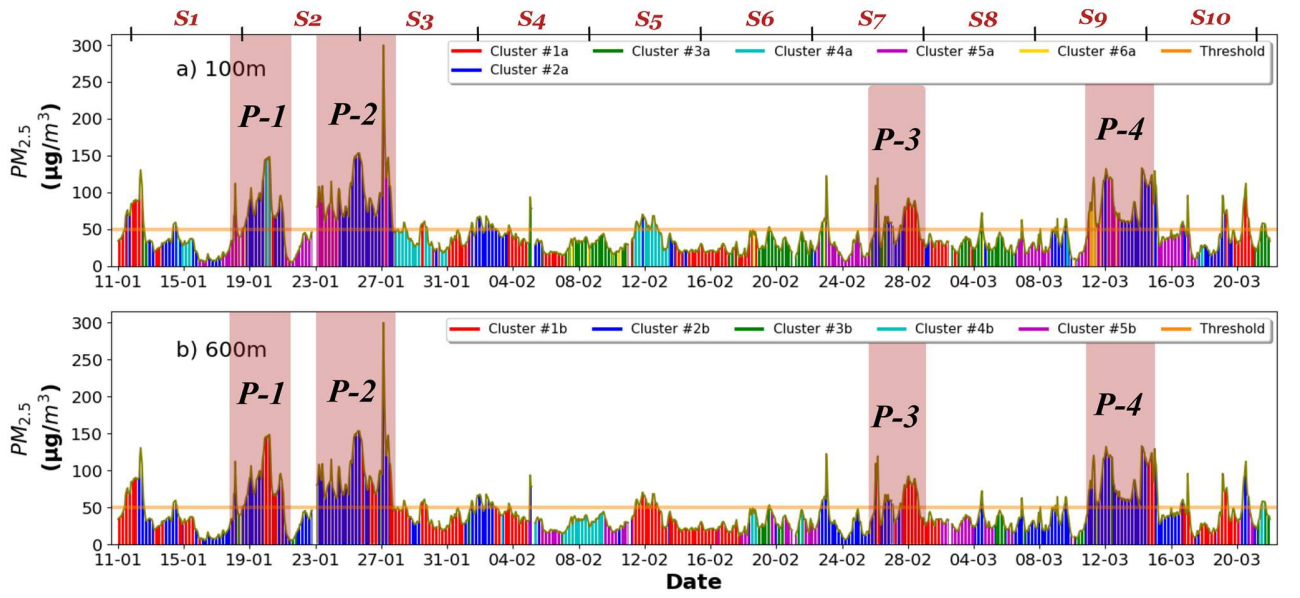

Figure 6: Hourly $PM_{2.5}$ concentrations colored as a function of the HYSPLIT cluster attribution for back-trajectories arriving at height of 100m and 600m a.g.l. Threshold (orange line) based on the specified Vietnam's standard for ambient air quality in 24-h (≥ 50 µg m^{-3}). S_1 - S_{10} represent the periods of time of the 10 weekly filter samples.

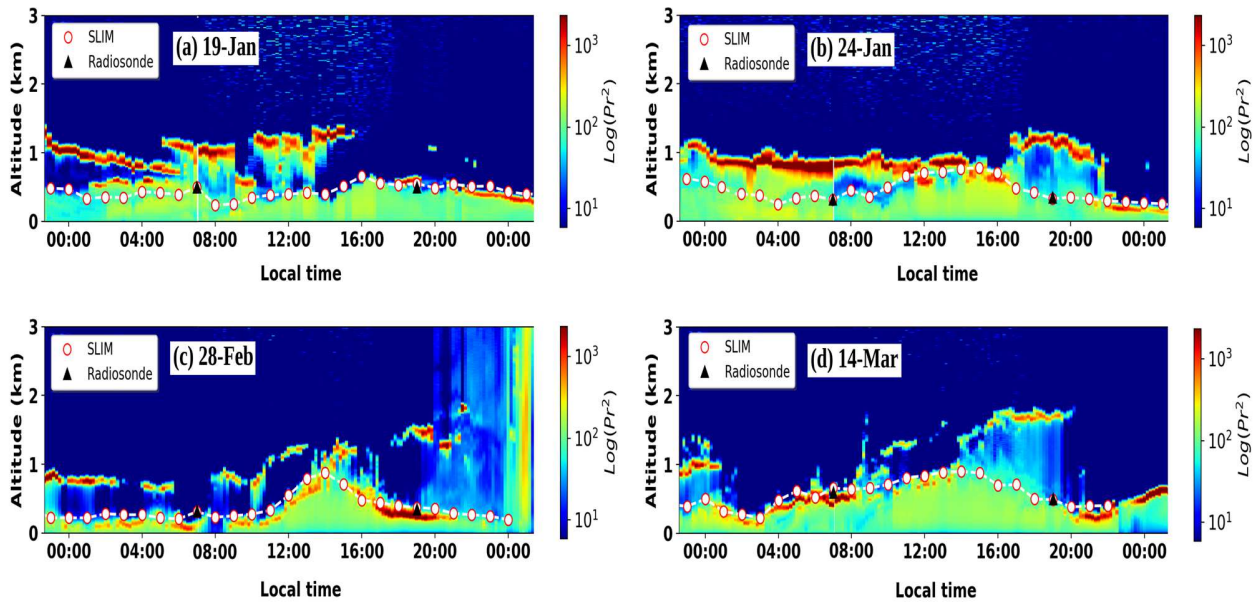

Figure 7: Time-height cross-sections of SLIM Lidar range-corrected signal (Pr^2) and time series of boundary-layer height (BLH) on (a) 19/01, (b) 24/01, (c), 28/02 and (d) 14/03. The BLH retrieved from SLIM (respectively radiosondes) profiles is represented as red circles (respectively black triangles).

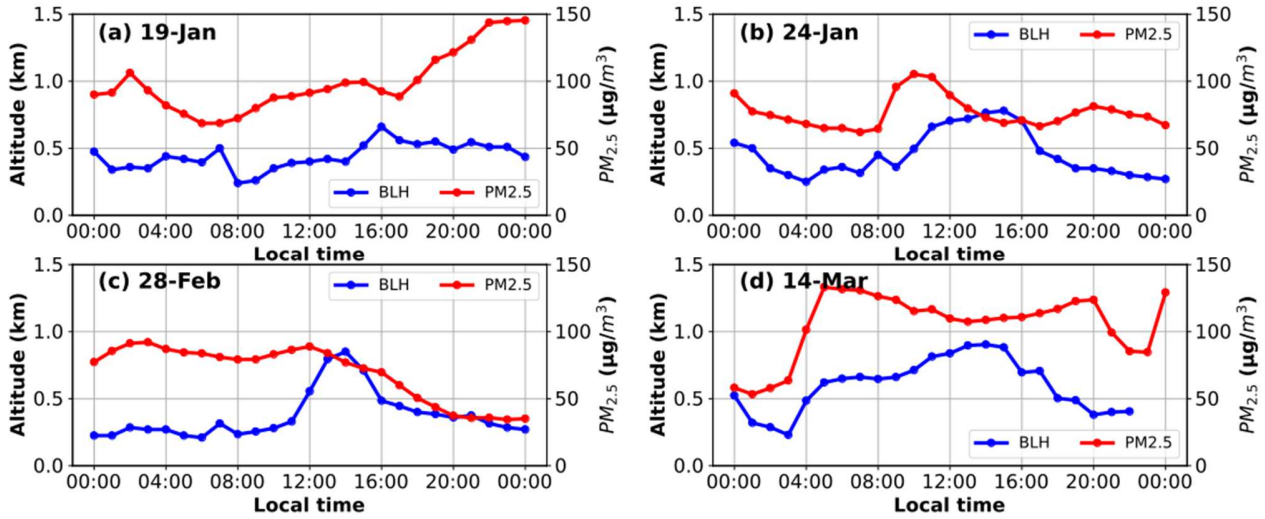

Figure 8: Hourly time series of boundary layer height (BLH) from the aerosol lidar and $PM_{2.5}$ concentrations on (a) 19/01, (b) 24/01, (c) 28/02 and (d) 14/03.

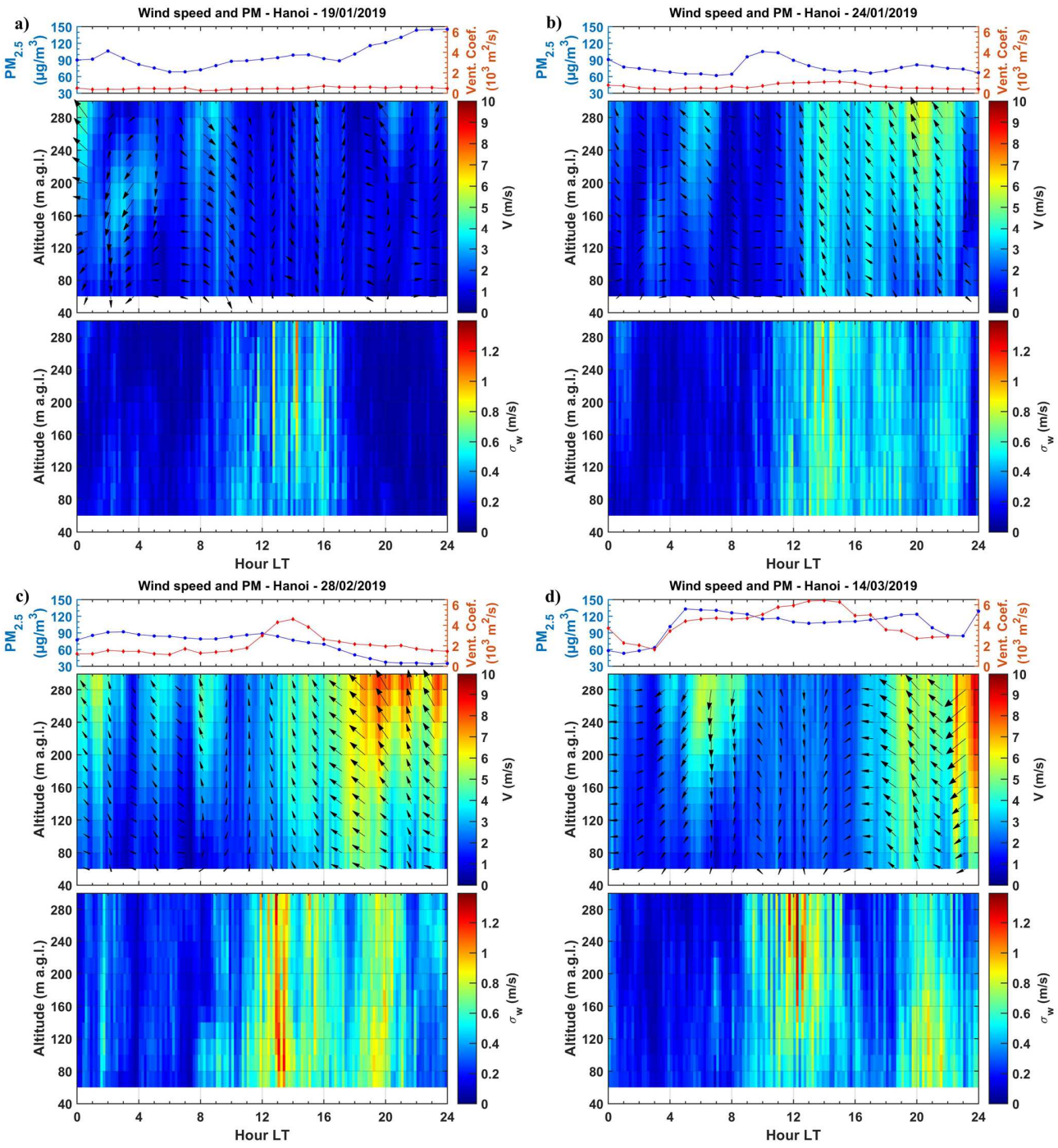

Figure 9: Time series of $PM_{2.5}$ concentration (upper) and time-height cross-sections of horizontal wind speeds (middle) and vertical mixing (below) measured by the Doppler Lidar on (a) 19/01, (b) 24/01, (c) 28/02 and (d) 14/03.

Key factors explaining severe air pollution episodes in Hanoi under the impact of the Northeast winter monsoon

Bao Anh Phung Ngoc[a,b], Hervé Delbarre[a], Karine Deboudt[a], Elsa Dieudonné[a], Dien Nguyen Tran[b], Son Le Thanh[b], Jacques Pelon[c], François Ravetta[c]

[a] *Laboratoire de Physique et Chimie Atmosphériques (LPCA), Université du Littoral Côte d'Opale, Dunkerque, France.*

[b] *Institute of Environmental Technology (IET), Vietnam Academy of Science and Technology, Hanoi, Vietnam.*

[c] *Laboratoire Atmosphère Milieux, Observations Spatiales (LATMOS), CNRS-INSU, Sorbonne Université, Université Versailles St Quentin, Paris, France.*

*Corresponding author: Phung Ngoc Bao Anh

E-mail addresses: anh-bao.phung-ngoc@univ-littoral.fr

Graphical abstract